JOURNAL OF AIRCRAFT
Vol. 37, No. 2, March–April 2000

Simulated Flowfields in Near-Ground Operation of Single- and Twin-Rotor Configurations

Ning Kang* and Mao Sun†
Beijing University of Aeronautics and Astronautics, 100083 Beijing, People's Republic of China

Numerical simulation with Navier–Stokes (N–S) equations is carried out for studying the flowfields of single, tandem, side-by-side, and coaxial rotors operating near the ground at low flight speeds. Source terms are introduced into the N–S equations to represent the rotor blades; therefore, only the flow scales of rotor far wake and ground boundary layer need to be resolved. Calculated results reveal the complex ground vortex phenomena produced by the interactions between the multiple wakes, the ground plane, and the incoming freestream. The effects of advance ratio, height above ground, as well as the rotor configuration, are analyzed.

Nomenclature

H	= height above ground
p	= pressure
R	= rotor radius
r	= radial station
S'_x, S'_y, S'_z	= source terms
u, v, w	= Cartesian velocity components
x, y, z	= Cartesian coordinates
x_c, y_c, z_c	= coordinates of the rotor center
μ	= advance ratio
ν	= kinematic viscosity
ρ	= density
ψ	= blade azimuth angle

Introduction

THE past two decades have seen an increased demand for helicopters to fly near the ground at very low speeds in both military and civilian applications. When a rotor in forward flight is near the ground, its wake impinges on the ground and then rolls up and, under the influence of incoming flow, forms a horseshoe-shaped vortex, the ground vortex, as in Fig. 1. This ground vortex will change the aerodynamic characteristics of the rotor. The flow environment becomes much more complex compared with that of flight out-of-ground effect. New aerodynamic phenomena, involving problems in balance, control, and stability, will arise. It is therefore important to investigate this area and clearly understand the characteristics of the ground vortex. The situation of a single rotor in forward flight near the ground was studied extensively (e.g., Refs. 1 and 2); however, few studies have been carried out for the cases of twin-rotor systems, such as coaxial, side-by-side, and tandem twin-rotor systems. For twin-rotor systems there are two wakes. When the two wakes impinge on the ground, under the influence of the incoming flow and the mutual influence between the two wakes, the resulting flowfield can be much more complex than that of single rotor operating near the ground. Little investigation has been carried out with regard to this problem. This paper is devoted to the investigation of the flowfield of the twin-rotor systems operating in the low-height and low-speed regime, using the method of Navier–Stokes (N–S) simulation.

One way of using the method of N–S simulation is to solve directly the flow dynamic equations with rotor blades as the inner boundary. Although this method could give detailed velocity field information near the rotor, it has to invoke the use of body-fitted curvilinear coordinates to follow the rotor geometry and to use very fine grids near the rotor surface in order to resolve the boundary-layer flow on the blade surfaces. For studying the ground vortex phenomena, the far wake and the boundary layer on the ground plane also need fine resolution. This requires very large computing power and a great deal of computer storage. There exists another way of using N–S equations, developed in Refs. 3 and 4, which introduces momentum sources into the N–S equations to represent the interaction between the rotors and the flowfield. This method gives up calculating the detailed flowfield near the blades and emphasizes the calculation of the far-field flow. Without the fine flow scale of blade boundary layer, there are only the relatively larger flow scales of the rotor wakes to be resolved. This will greatly simplify the process of numerical calculation and is also very suitable for the simulation of rotor far wakes and their interactions with other objects. This procedure has been used successfully in the analysis of the flowfield and performance of a single helicopter rotor in hover[3] and in forward flight.[4] Recently, the authors of this paper have used it to simulate the flowfield of a single rotor in ground effect and obtained very good results.[2] In the present paper this method is used to study the flowfields of the tandem, side-by-side, and coaxial rotor configurations in ground effect at low flight speeds. For comparison, the same results of single rotor are also presented.

Computational Method

The steady, incompressible, laminar N–S equations in Cartesian coordinates (see Fig. 2) are as follows:

Continuity:

$$\frac{\partial u}{\partial x}+\frac{\partial v}{\partial y}+\frac{\partial w}{\partial z}=0 \tag{1}$$

Momentum:

$$\rho\left(u\frac{\partial u}{\partial x}+v\frac{\partial u}{\partial y}+w\frac{\partial u}{\partial z}\right)=-\frac{\partial p}{\partial x}+\rho\nu\left(\frac{\partial^2 u}{\partial x^2}+\frac{\partial^2 u}{\partial y^2}+\frac{\partial^2 u}{\partial z^2}\right)+S'_x \tag{2}$$

$$\rho\left(u\frac{\partial v}{\partial x}+v\frac{\partial v}{\partial y}+w\frac{\partial v}{\partial z}\right)=-\frac{\partial p}{\partial y}+\rho\nu\left(\frac{\partial^2 v}{\partial x^2}+\frac{\partial^2 v}{\partial y^2}+\frac{\partial^2 v}{\partial z^2}\right)+S'_y \tag{3}$$

$$\rho\left(u\frac{\partial w}{\partial x}+v\frac{\partial w}{\partial y}+w\frac{\partial w}{\partial z}\right)=-\frac{\partial p}{\partial z}+\rho\nu\left(\frac{\partial^2 w}{\partial x^2}+\frac{\partial^2 w}{\partial y^2}+\frac{\partial^2 w}{\partial z^2}\right)+S'_z \tag{4}$$

In the preceding equations the particularly noteworthy terms are the source terms S'_x, S'_y, S'_z. They denote the force per unit volume caused by the action of the rotor on the flows and are distributed in regions occupied by rotors. The lifting-line theory is invoked to calculate the aerodynamic force on the rotor wakes. Its reacting

Received 27 May 1998; revision received 23 April 1999; accepted for publication 30 August 1999.

*Associate Professor, Institute of Fluid Mechanics.
†Professor, Institute of Fluid Mechanics.

force is the force of rotor acting on the flow. This force is then converted to be the sources added to the momentum equations. The readers are referred to Refs. 3 and 4 for a detailed description of this method. The governing equations are solved using a finite volume method, and the coupling of the velocity and the pressure is done via the SIMPLER algorithm.[5]

The computational domain is a cuboid containing the rotor. The surface of the rotor blades is no longer the boundary because the rotor was replaced by the momentum sources. The boundary conditions for the present problems are as follows: on the ground plane, nonslip conditions are prescribed; and on the far boundaries either incoming flow or extrapolation conditions are prescribed.

Results and Discussion

Calculations and analyses are carried out in this paper for a single-rotor configuration three twin-rotor configurations: 1) side-by-side rotors, 2) tandem rotors, and 3) coaxial rotors. For side-by-side rotors the distance between the rotor centers is $2.2R$. For tandem rotors the longitudinal distance between the rotor centers is $1.4R$, and the vertical distance is $0.2R$. For coaxial rotors the vertical distance between the rotor centers is $0.2R$. In the present study the model rotor used for ground-effect study in Ref. 1 is chosen. The rotor has four blades of 1.219 m in radius and rotates at 47.15 rad/s. The blade linear twist angle is -8 deg, and the blade pitch at the root is 18 deg. The rotor disk angle of attack is zero. The blade section is a NACA 0012 airfoil. For the coaxial rotor configuration each rotor has two blades. Flight conditions considered are as follows: three advance ratios $\mu = 0.03$, 0.045, and 0.06 for each of the three heights above ground $H = 0.46R$, $0.88R$, and ∞.

Grid Study and Validation by Experiment

Detailed grid sensitivity study is performed for the single-rotor configuration at typical flight conditions (for the single rotor, experimental flow visualization data are available for comparison). Two computational domains (domain I and domain II) of different size and four grids total are considered. For domain I the upstream boundary is $11R$, the downstream boundary $17R$, the left- or right-side boundary $13R$, and the top boundary $15R$ from the rotor center. With this computational domain computations are done for three grids: grid 1, $45 \times 29 \times 42$; grid 2, $72 \times 45 \times 66$; and grid 3, $106 \times 66 \times 96$. The grid points are condensed near the ground plane and near the rotor disk plane and become coarser away from them. Figure 2 shows the calculated induced velocity distributions along the longitudinal symmetric axis of the rotor, and Fig. 3 shows some samples of the flowfields in the rotor longitudinal plane of symmetry. For grid 1 and grid 2 there is some difference between the calculated induced velocity distributions (Fig. 2), but both grids capture the ground vortex (because the ground vortex is of large scale), giving approximately the same location of vortex center and vortex size (Fig. 3). The induced velocity distribution calculated using grid 3 is also shown in Fig. 2, and it is close to that calculated using grid 2 (the flow picture of the ground vortex calculated using grid 3, not shown here, is very similar to that calculated using grid 2). For domain II the upstream, downstream, left- or right-side, and top boundaries are $14R$, $24R$, $18R$, and $20R$ from the rotor center, respectively. The grid used for this domain is $80 \times 49 \times 73$ (grid 4). To see the effect of domain size, this grid is made identical with grid 2 in the common part of domain I and domain II. From Fig. 2 one can see that the induced velocity distribution calculated using grid 4 is very close to that of grid 2 (the flow picture of ground vortex calculated using grid 4, not shown here, is very similar to that calculated using grid 2). This shows that increasing the computational domain size from that of domain I produces negligible effect. From the preceding results the conclusion is made that grid 2 is proper for the single rotor in the present study. Some samples of the calculated flow patterns of the ground vortex using grid 2 are compared with smoke visualization pictures[1] in Fig. 4. One can see that the calculated and experimental flow patterns are in good agreement.

For the other rotor configurations the grids employed in the present study are chosen under the guidance of the preceding results. For the tandem rotors, the grid is $92 \times 53 \times 66$ (compared with grid 2, 20, and 8 points are used in x and y directions, respectively, because grid clustering is needed for another rotor). For the coaxial rotors the grid is $72 \times 53 \times 66$. For the side-by-side rotors the grid is $72 \times 45 \times 52$ for the left half of the computational domain

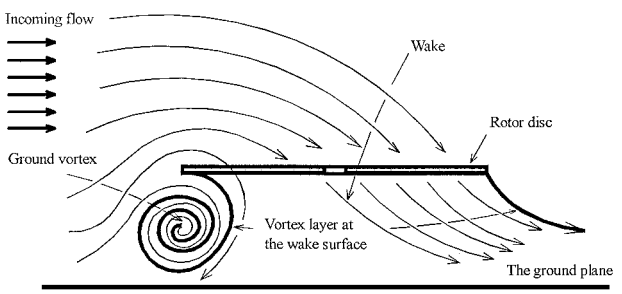

Fig. 1 Illustration of the flowfield in the longitudinal symmetry plane of a rotor in ground effect.

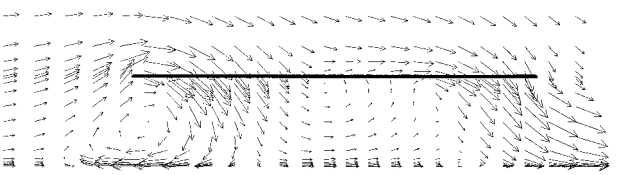

Grid 1

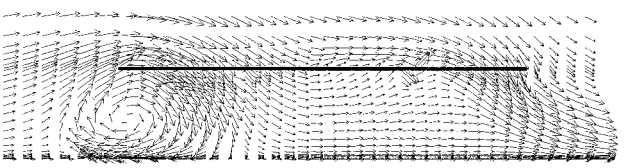

Grid 2

Fig. 3 Velocity fields at longitudinal cross section of symmetry, single rotor, $H = 0.46R$, and $\mu = 0.045$.

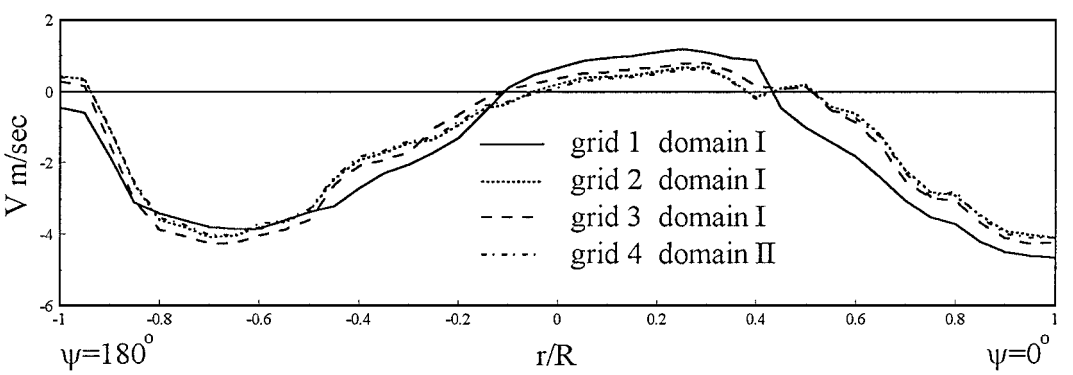

Fig. 2 Induced velocity distributions for different grids and computational domains, single rotor, $H = 0.46R$, and $\mu = 0.045$.

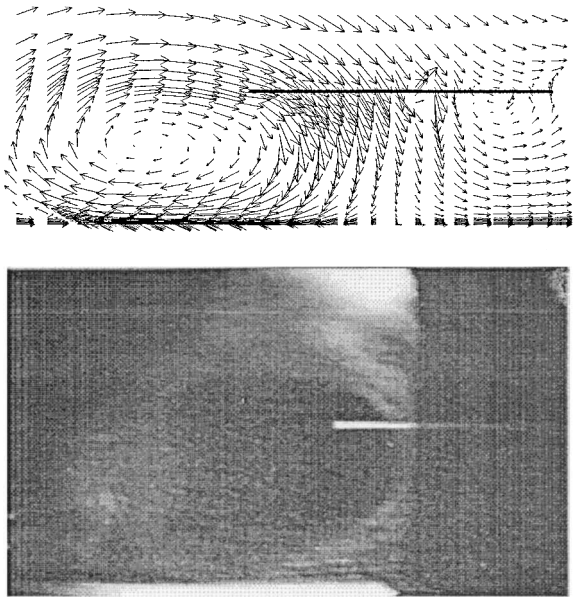

μ = 0.03

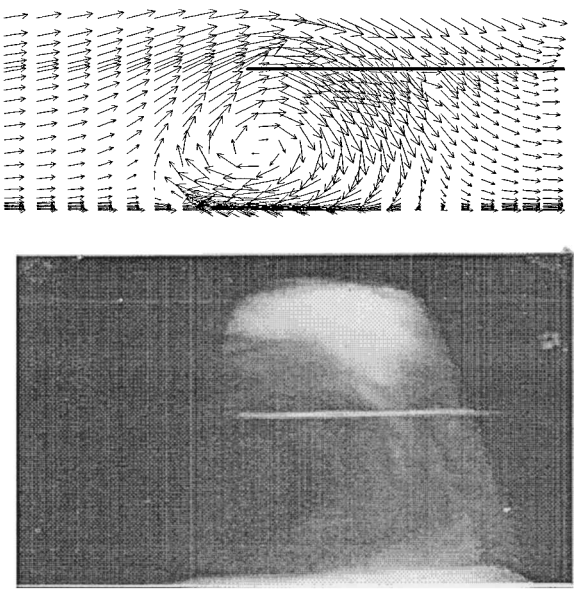

μ = 0.045

Fig. 4 Computational and experimental flowfield of a single rotor in the longitudinal cross section of symmetry with different μ at $H = 0.46R$.

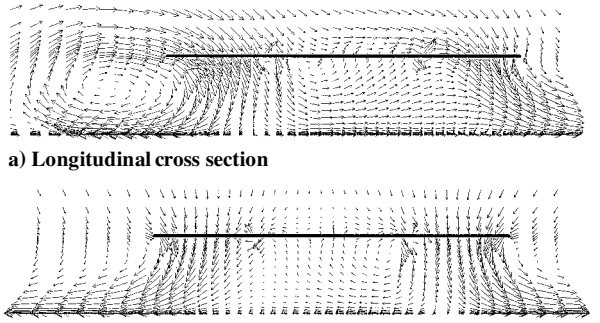

a) Longitudinal cross section

b) Lateral cross section

Fig. 5 Velocity fields at longitudinal and lateral cross sections, single rotor, $H = 0.46R$, and $\mu = 0.03$.

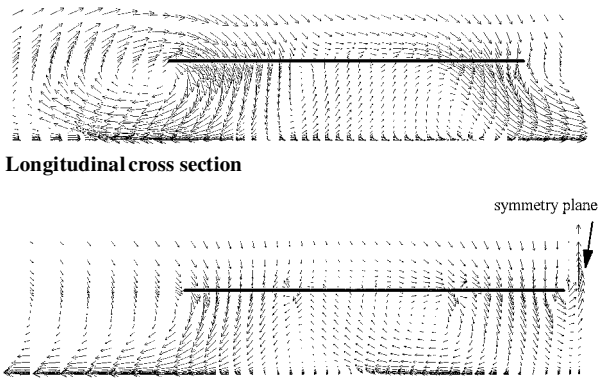

Longitudinal cross section

Lateral cross section

Fig. 6 Velocity fields at longitudinal and lateral cross sections, side-by-side rotors, $H = 0.46R$, and $\mu = 0.03$.

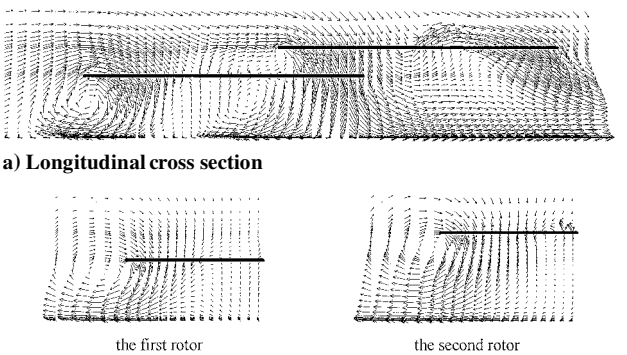

a) Longitudinal cross section

b) Lateral cross section (left half)

Fig. 7 Velocity fields at longitudinal and lateral cross sections, tandem rotors, $H = 0.46R$, and $\mu = 0.03$.

(symmetry condition is employed between the two side-by-side rotors). For all cases there are more than 12 grid points in the ground boundary layer.

Flowfield Description

From our calculated results the flowfields of the coaxial rotors (with two two-blade rotors) were found to be very similar to that of a single rotor with four blades. Therefore, only the results for the tandem, side-by-side, and single-rotor configurations will be described in detail here. Some examples of the coaxial rotor flowfields compared with that of the single rotor will be given later in this section.

Figures 5–7 present the velocity fields for the three rotor configurations at $\mu = 0.03$ and $H = 0.46R$. The vector velocity field is drawn at longitudinal cross section ($z = z_c$) and lateral cross section ($x = x_c$). Flowfields of the rotors without ground effects were also calculated but are not shown here because of the limitation of space. Because of the presence of the ground, the flowfields are significantly different from that without ground effect. For the case without ground effect, the flow under the rotor is mainly downward and inclined to the back and is similar to a freejet that is blown downstream. For the case with ground effect, the forward part of the rotor wake impinges on the ground and then rolls up and, because of the incoming flow, forms a ground vortex. This is true for all of the rotor configurations. For cases of single-rotor and side-by-side configurations (Figs. 5 and 6), the part of wake under the center of the rotor is reflected from the ground and moves upward through the middle and rear part of the rotor plane. But for the case of the tandem configuration (Fig. 7), there is another vortex under the center of the forward rotor (Fig. 7a). The second ground vortex looks weaker than the first. The velocity field in the middle and rear part of the forward rotor is greatly influenced by the second ground vortex and becomes much more complicated. For the case of single rotor, the ground vortex center in the longitudinal symmetric plane is a little upstream of the rotor leading edge (Fig. 5). For the case of the side-by-side configuration (Fig. 6), the center of the ground vortex is higher and closer to the rotor leading edge than that of

single rotor, and the vortex is a little larger in size, which may be because the side-by-side presence of another rotor would force a larger part of wake to flow forward. For the case of the tandem configuration (Fig. 7), the first ground vortex is under the rotor leading edge and smaller in size than that of the single rotor. In this case, because of the tandem presence of the second rotor, the flow that enters into the forward rotor will be less; hence, the part of wake of the forward rotor following upstream becomes less than that of single rotor, resulting in a smaller ground vortex.

Figures 8–10 show the velocity fields at a higher advance ratio. At this advance ratio the ground vortex location is moved downstream under the front part of the rotor, and its size becomes smaller. Our calculated results show that when the advance ratio increases the ground vortex will move downstream, become smaller, and finally disappear. For the case of the single rotor, it disappears at about $\mu = 0.06$; for the case of side-by-side rotors, at about $\mu = 0.065$; for the case of tandem rotors, at about $\mu = 0.055$. In addition, the upward velocity in the middle and rear part of the rotor which is caused by wake reflection decreases with the increase of advance ratio.

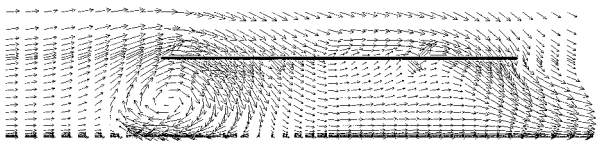

Longitudinal cross section

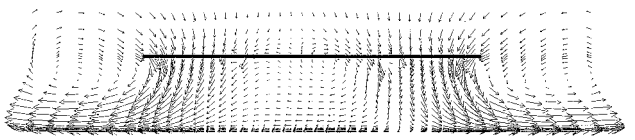

Lateral cross section

Fig. 8 Velocity fields at longitudinal and lateral cross sections, single rotor, $H = 0.46R$, and $\mu = 0.045$.

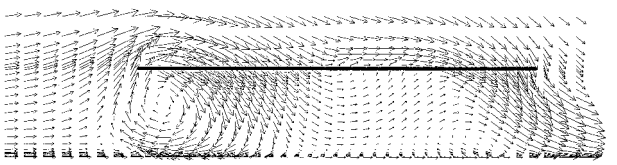

Longitudinal cross section

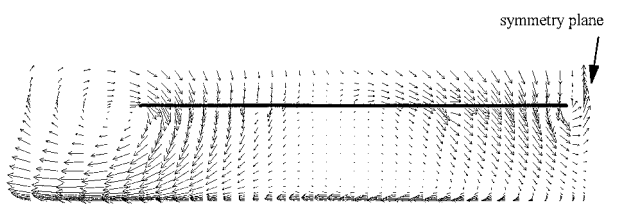

Lateral cross section

Fig. 9 Velocity fields at longitudinal and lateral cross sections, side-by-side rotors, $H = 0.46R$, and $\mu = 0.045$.

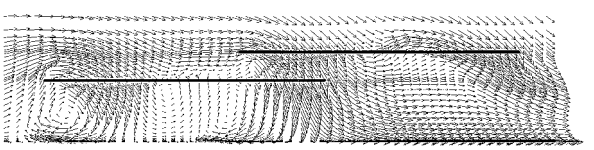

a) Longitudinal cross section

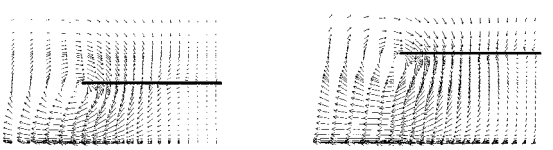

b) Lateral cross section (left half)

Fig. 10 Velocity fields at longitudinal and lateral cross sections, tandem rotors, $H = 0.46R$, and $\mu = 0.045$.

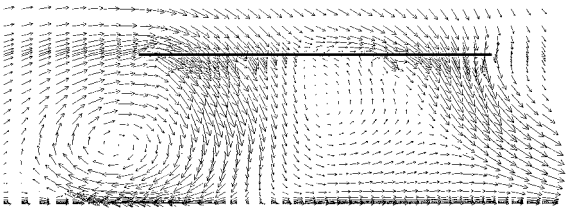

Fig. 11 Velocity fields at longitudinal cross section, single rotor, $H = 0.88R$, and $\mu = 0.03$.

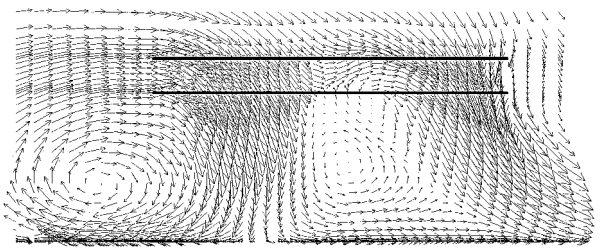

Fig. 12 Velocity fields at longitudinal cross section, coaxial rotors, $H = 0.88R$, and $\mu = 0.03$.

Figure 11 shows a sample of the flowfields at a larger height above ground for $\mu = 0.03$. When H is larger, the vortex is moved downstream, its strength is weakened, and is more distant from the rotor plane. From our calculated results (not shown here), for a higher H the ground vortex emerges at a smaller advance ratio while it disappears at a smaller advance ratio as well.

A sample of the flowfields of the coaxial rotor is shown in Fig. 12. Compare the flowfield in Fig. 12 with that in Fig. 11; the flow patterns of the four-blade single rotor and the coaxial rotors (two two-blade rotors) are similar.

Induced Velocity Distribution

From the flowfields just discussed one can see that as the advance ratio increases the ground vortex moves from in front of the rotor leading edge to under the rotor and the reflection of the wake from the ground plane becomes weak. These may cause the induced velocity distribution on the rotor plane to change significantly with the variation of μ. The induced velocity distributions at the rotor plane for single rotor, side-by-side rotors, tandem rotors, and coaxial rotors at different advance ratios are shown in Figs. 13–15. They are given at $\psi = 0$, 90, 180, and 270 deg i.e., along the rotor longitudinal and lateral axes. For the case of the single rotor, at $\mu = 0.03$ the ground vortex is in front of the rotor leading edge (Fig. 5a), and at $\mu = 0.06$ it moves to under the rotor disc. The effect of this movement is reflected in the induced velocity distribution in Fig. 13. The induced velocity distribution varies greatly for these two advance ratios at the front part of the rotor (i.e., in the vicinity of $\psi = 180$ deg and $r \cong 0.5$–1). The induced velocity distribution around the rotor center also changes noticeably with the variation of μ (see Fig. 13, at $r = 0$–0.4, $\psi = 90$ and 270 deg) because the extent of the wake reflecting varies with advance ratio. For the case of side-by-side rotors, as μ varies, the variations of the location of the ground vortex and the extent of wake reflection are similar to that of the single rotor; therefore, the induced velocity distribution (Fig. 14) varies with μ in a way similar to that of single rotor. However, in the vicinity of $\psi = 90$ deg, $r = 0.7$–1.0, the variation of the induced velocity distribution with μ is larger than that of single rotor because of the presence of another rotor. For the tandem configuration Fig. 15 shows the induced velocity distributions for the first and the second rotor. For the first rotor (Fig. 15a) near the rotor leading edge ($\psi = 180$ deg, $r = 0.6$–1.0), the induced velocity distribution varies with μ in a similar way to that of single rotor and side-by-side rotors. But on the rest of the longitudinal axis ($\psi = 0$–180 deg), unlike that

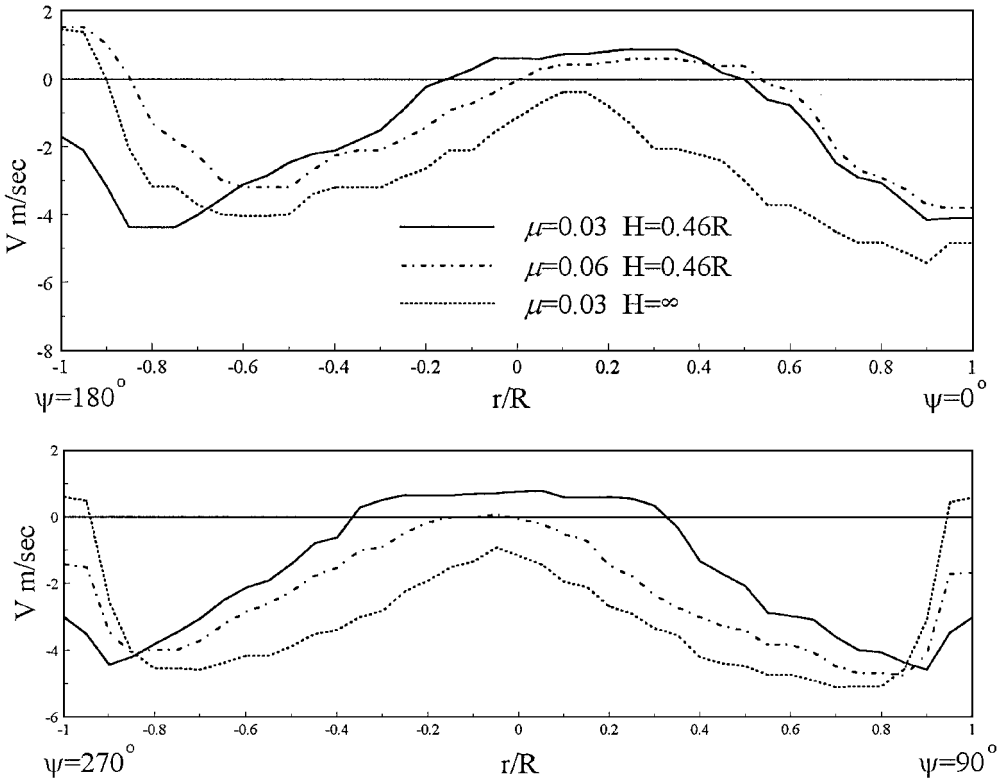

Fig. 13 Induced velocity distribution, single rotor.

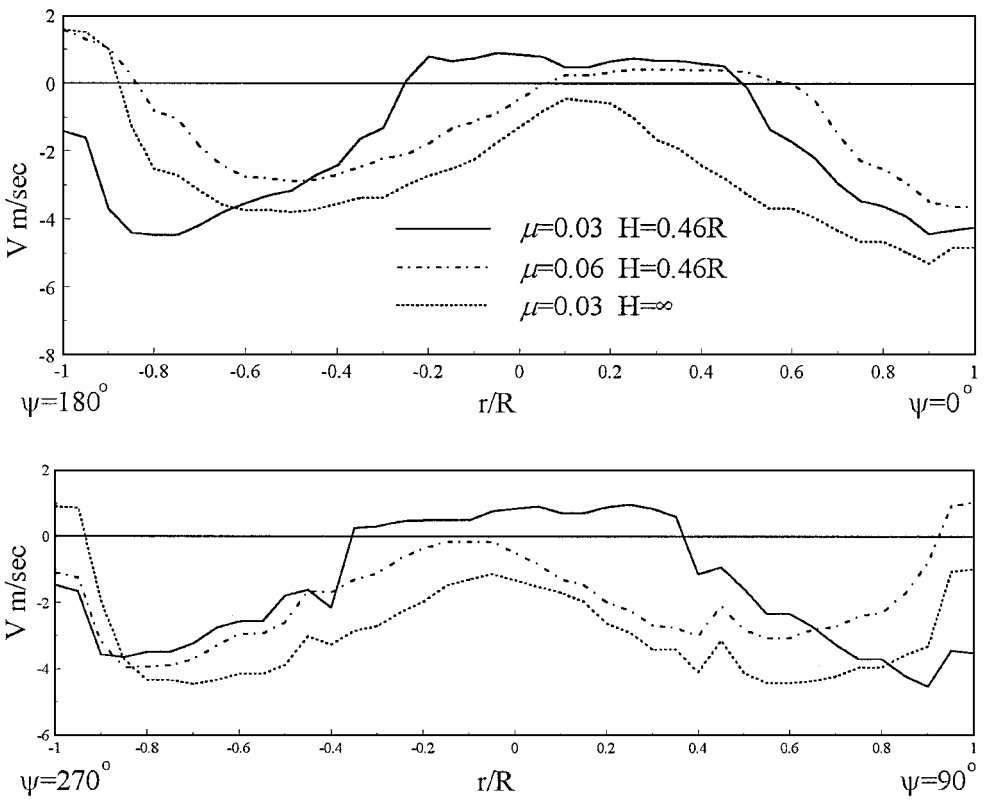

Fig. 14 Induced velocity distribution, side-by-side rotors.

of single rotor and side-by-side rotors, the induced velocity distribution also varies greatly with μ. This is because of the movement of the second ground vortex, which moves under the first rotor as μ varies (see Figs. 7a and 10a). For the second rotor, for most of the longitudinal (and lateral) axes (Fig. 15b), the induced velocity distribution varies much less as μ increases, compared with that of the first rotor. This may be because the second rotor is far away from the two ground vortices. For the two-blade coaxial rotors the induced velocity distribution of the twin rotors varies with μ in a similar way to that of the four-blade single rotor.

To show the effect of height above ground, the induced velocity distributions for $H = \infty$ at $\mu = 0.03$ are included in Figs. 13–15, respectively, for the different configurations. For the single rotor (Fig. 13), comparing the induced velocity distribution of $H = 0.46R$ and ∞, it is clear that the ground vortex and the reflection of the wake from the ground plane greatly alter the induced velocity distribution

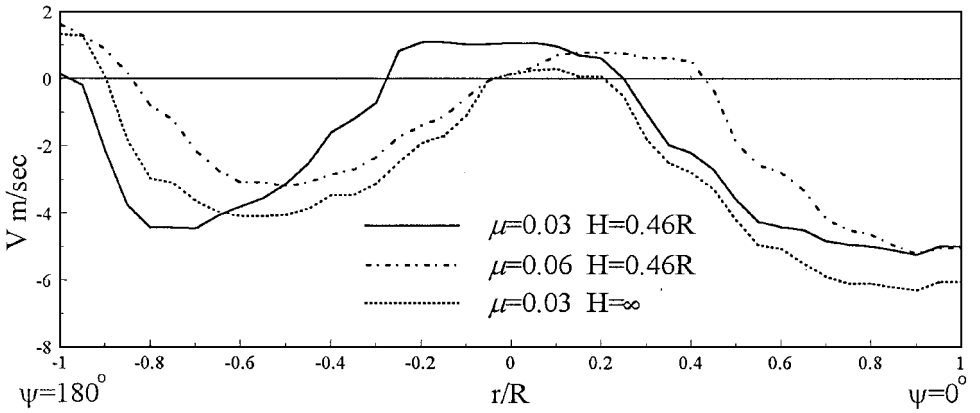

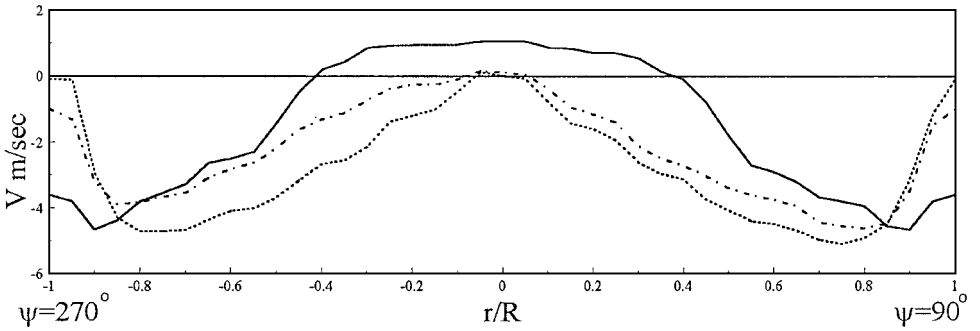

a) At the first rotor

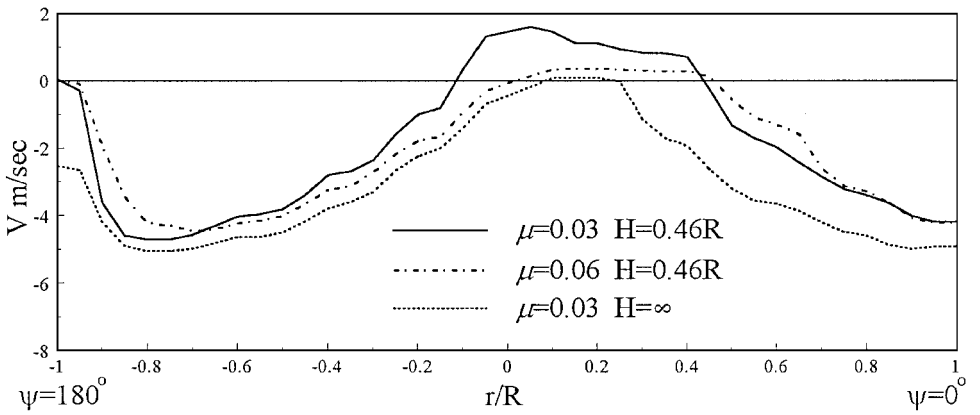

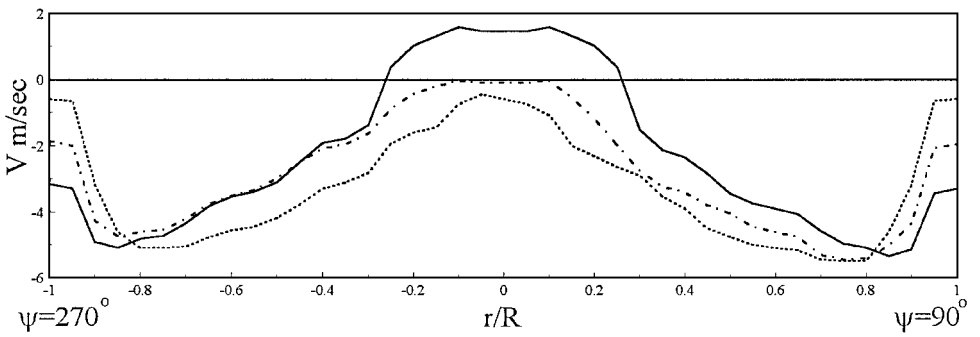

b) At the second rotor

Fig. 15 Induced velocity distribution, tandem rotors.

at the rotor disc. Unlike the influence caused by varying μ, the effect here takes place not only in the front part of the rotor, but also in the middle and the rear part of the rotor. The variation in the front part of the rotor is caused by the effect of the ground vortex, whereas the variation in the rest part is caused by the effect of the ground plane, which is equivalent to adding an upward velocity to the rotor disc. The closer the rotor is to the ground, the greater the upward velocity. From Figs. 14 and 15 for the tandem and side-by-side configurations, the induced velocity distributions vary with H in a way similar to that of a single rotor.

Conclusions

1) When single, side-by-side, tandem, and coaxial rotors are operating near the ground at low advance ratios, the forward part of the rotor wake, after impinging on the ground plane, will flow forward and then roll up, forming a horseshoe vortex, ground vortex, around

the rotors. For the single rotor, side-by-side rotors, and coaxial rotors, the wake reflects from the ground and gives an upward velocity in the middle and rear part of rotors. For tandem rotors there is another ground vortex under the rear part of the forward rotor. The second vortex greatly influences the velocity field in the middle and rear part of the forward rotor. With the increase of advance ratio and height above ground, the ground vortices move downstream, become smaller, and finally disappear.

2) For single rotor and side-by-side rotors, at the front and in the middle of the rotor the induced velocity distribution varies greatly with advance ratio. For the first rotor of tandem rotors, the induced velocity distribution varies greatly with advance ratio, near the rotor leading edge, and on the rest part of the rotor as well. For the second rotor the induced velocity distribution varies much less with advance ratio. For coaxial rotors the induced velocity distribution that varies with advance ratio is similar to that of a single rotor.

3) For all configurations the induced velocity distribution varies with height above ground greatly, not only in the front part of the rotor but also in the rest part of the rotor.

Acknowledgment

This work was supported by the National Natural Science Foundation of China under the Contract 19725210.

References

[1] Sun, M., "A Study of Helicopter Rotor Aerodynamics in Ground Effect at Low Speeds," Ph.D. Dissertation, Dept. of Mechanical and Aerospace Engineering, Princeton Univ., Princeton, NJ, Aug. 1983.

[2] Kang, N., and Sun, M., "Prediction of the Flow Field of a Rotor in Ground Effect," *Journal of the American Helicopter Society*, Vol. 42, No. 2, 1997, pp. 195–198.

[3] Rajagopalan, R. G., and Lim, C. K., "Laminar Flow Analysis of a Rotor in Hover," *Journal of the American Helicopter Society*, Vol. 6, No. 1, 1991, pp. 12–23.

[4] Rajagopalan, R. G., and Mathur, S. R., "Three Dimensional Analysis of a Rotor in Forward Flight," *Journal of the American Helicopter Society*, Vol. 38, No. 3, 1991, pp. 14–25.

[5] Patankar, S. V., *Numerical Heat Tranfer and Fluid Flow*, Hemisphere, New York, 1980, Chap. 6, pp. 130–157.